The H-NOX protein structure adapts to different mechanisms and functions in sensors interacting with nitric oxide

Byung-Kuk Yoo[a,1], Sergei G. Kruglik[b], Jean-Christophe Lambry[a], Isabelle Lamarre[a], C. S. Raman[c], Pierre Nioche[d,e] and Michel Négrerie[a,*]

[a]Laboratoire d'Optique et Biosciences, INSERM U-1182, Ecole Polytechnique, 91120 Palaiseau, France.
[b]Laboratoire Jean Perrin, Institut de Biologie Paris-Seine, Sorbonne Université, CNRS, 75005 Paris, France.
[c]Department of Pharmaceutical Sciences, School of Pharmacy, University of Maryland, Baltimore, Maryland 21201, USA.
[d]Environmental Toxicity, Therapeutic Targets, Cellular Signaling and Biomarkers, UMR S1124, Centre Universitaire des Saints-Pères, Université Paris Descartes, 75006 Paris, France.
[e]Structural and Molecular Analysis Platform, BioMedTech Facilities, INSERM US36-CNRS-UMS2009, Paris Université, Paris, France.

[1]Present address: Thermo Fisher Scientific, New Jersey, USA.

[*]To whom correspondence may be addressed. Email: michel.negrerie@polytechnique.edu

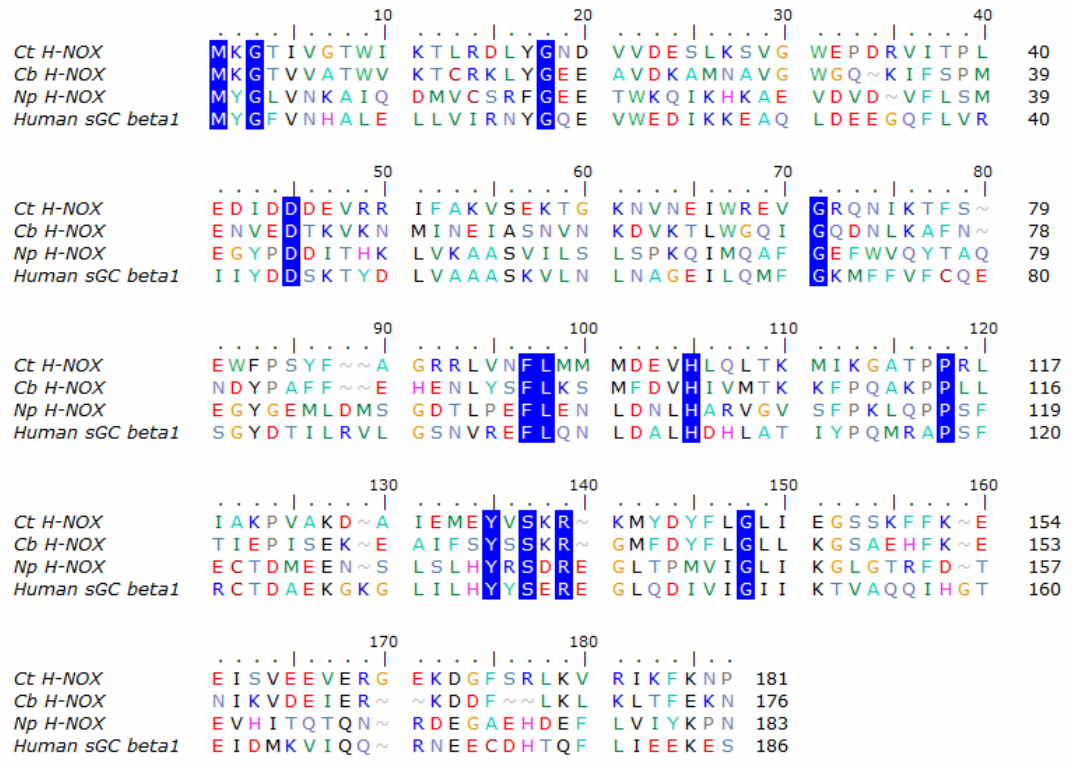

Figure S1. Sequence alignment of three H-NOX domains and human sGC β1. Sequence numbering is that of guanylate cyclase. Residues with absolute identity in the alignment are represented by blue blocks. The histidine residue coordinating the heme is represented by red block. These H-NOX share 18 % (*Ct*), 16 % (*Np*) and 40 % (*Cb*) sequence identity with the heme domain of human sGC. Accession numbers are from Pubmed as follows: *Ct* H-NOX [*Caldanaerobacter tengcongensis*, gi55670808], *Cb* H-NOX [*Clostridium botulinum*, gi148381498], *Np* H-NOX[*Nostoc punctiforme*, gi23129606], and Human β1 [*Homo sapiens*, gi2746083]. Alignments were generated using the BioEdit program.

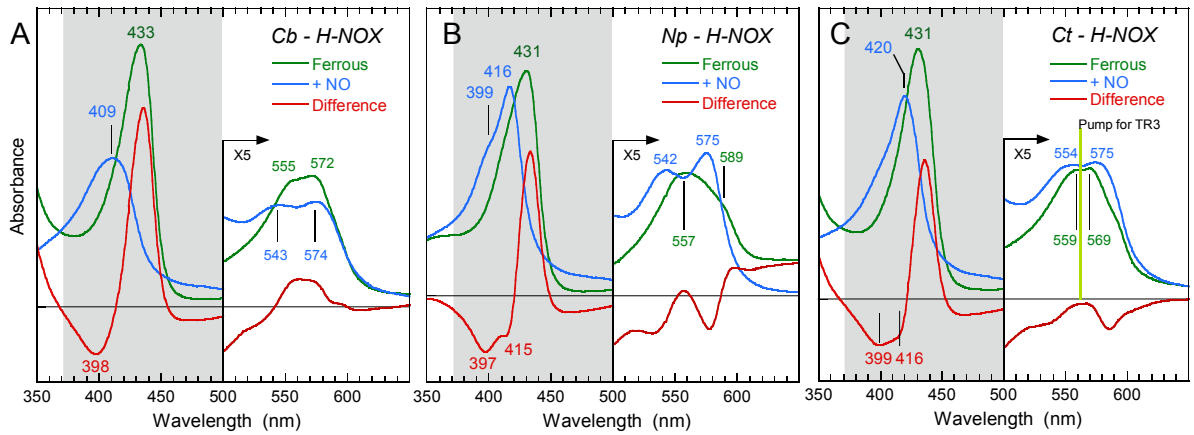

Figure S2. Electronic absorption spectra of unliganded and NO-bound *Cb* H-NOX (**A**), *Np* H-NOX (**B**) and *Ct* H-NOX (**C**) bacterial sensors at 20 °C. The difference spectra unliganded *minus* NO-liganded are calculated. The colored area represents the wavelength range probed by time-resolved spectroscopy. For *Ct* H-NOX the position of the Raman photodissociating pulse is indicated. NO at 10 % in the gas phase into the cell leads to [NO] = 200 µM in solution. Optical pathlength = 1 mm.

NO and heme dynamics in *Clostridium botulinum* H-NOX

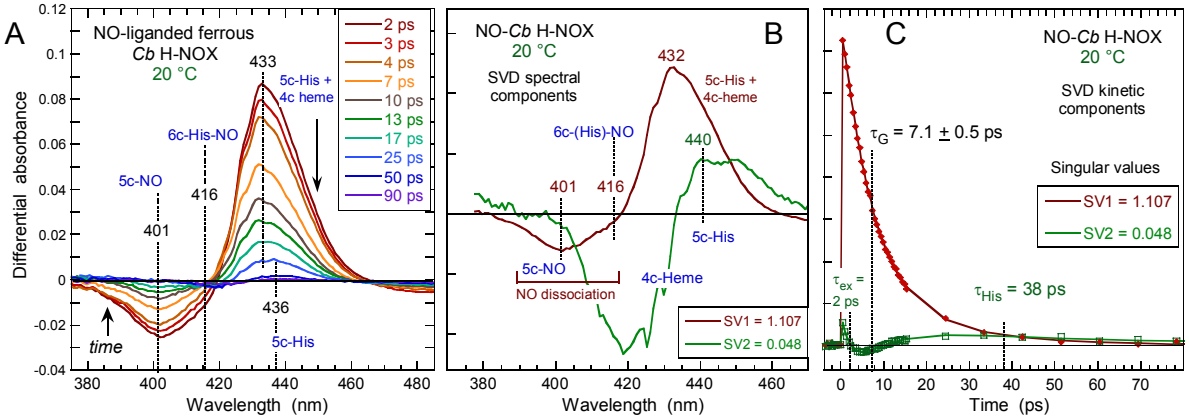

Figure S3. Interaction of NO with *Cb* H-NOX at T = 20 °C. **A**: Raw transient spectra a selected time delays after NO photodissociation. **B**: Spectral components from the SVD analysis of the time-wavelength matrix. **C**: Associated SVD kinetic components describing the evolution of the SVD spectral components.

Table S1. Time constants and relative amplitudes from fitting the SVD kinetics for *Cb* H-NOX.

T	SVD comp	Singular value	Excited states decay	NO geminate rebinding		His rebinding	constant (A_0)
			τ_{ex} (A_{ex})	τ_{G1} (A_1)	τ_{G2} (A_2)	τ_3 (A_3)	
4 °C	SVD1	1.461	1.3 ps (*0.10*)	6.7 ps (*0.71*)	23 ps (*0.18*)	–	*0.01*
	SVD2	0.096	2.1 ps (*0.31*)	6.5 ps (*0.45*)	–	34 ps (*0.20*)	*0.04*
20 °C	SVD1	1.107	1 ps (*0.06*)	7.1 ps (*0.81*)	24 ps (*0.13*)	–	*<0.01*
	SVD2	0.048	2.5 ps (*0.45*)	7.8 ps (*0.41*)	–	38 ps (*0.13*)	*<0.01*
40 °C	SVD1	0.976	1.2 ps (*0.14*)	6.9 ps (*0.76*)	23 ps (*0.09*)	–	*<0.01*
	SVD2	0.058	2.7 ps (*0.51*)	6.8 ps (*0.42*)	–	31 ps (*0.04*)	*0.03*

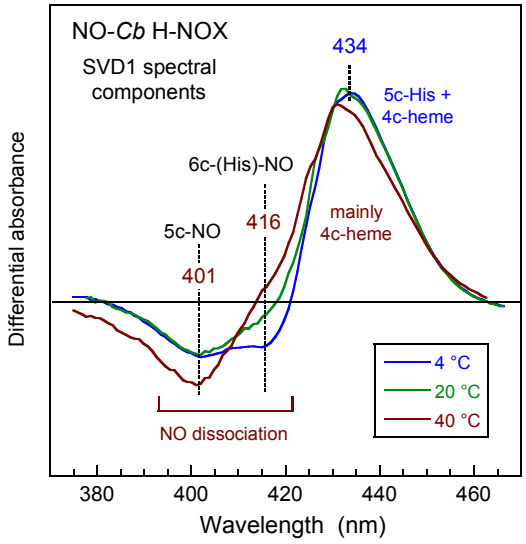

Figure S4. Comparison of the SVD1 spectral component at three temperatures for *Cb* H-NOX.

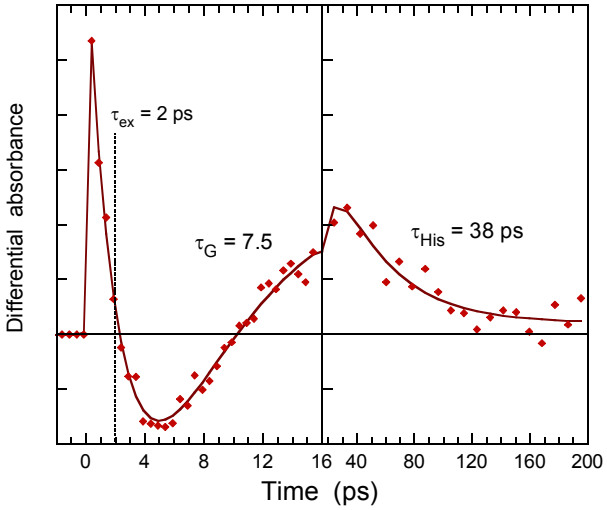

Figure S5. Enlarged view of the SVD2 kinetics for *Cb* H-NOX at T = 20 °C which describes the His rebinding (τ_{His}). The sign of its amplitude is opposite to that of NO rebinding (τ_G).

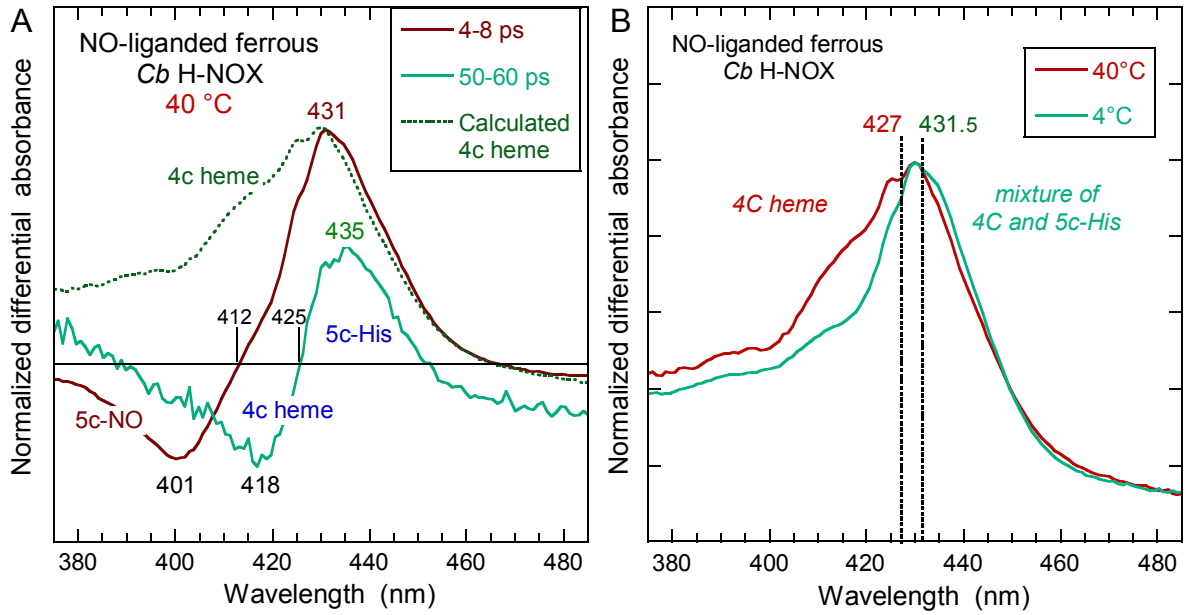

Figure S6. A: The difference transient spectrum at +50–60 ps (averaged) is compared to that at +4–8 ps (normalized at their bleaching minimum). The calculated spectrum of 4c heme at 40 °C (dotted dark green) is added for comparison. Its inverted rising side (400 – 420 nm) corresponds to the bleaching at +50 ps whereas its falling side (430 – 460 nm) corresponds to the induced absorption at +4 ps. Proximal His rebinding takes place at time longer (τ_{His} = 35 ± 4 ps; Fig. 3C-F and S5) than NO rebinding (τ_G = 7 ps). **B:** Absolute spectra of the products at Δt = +4 ps after photodissociation of NO at 4 °C and 40 °C. These spectra were calculated from raw data by subtracting the weighted spectrum of NO-liganded *Cb* H-NOX which is not photodissociated (~90%) from the absolute spectrum measured at +4 ps. The difference of the Soret band at both temperatures appears clearly, even if some 5c-His contribution is still present at 40 °C.

NO and heme dynamics in *Nostoc punctiforme* H-NOX

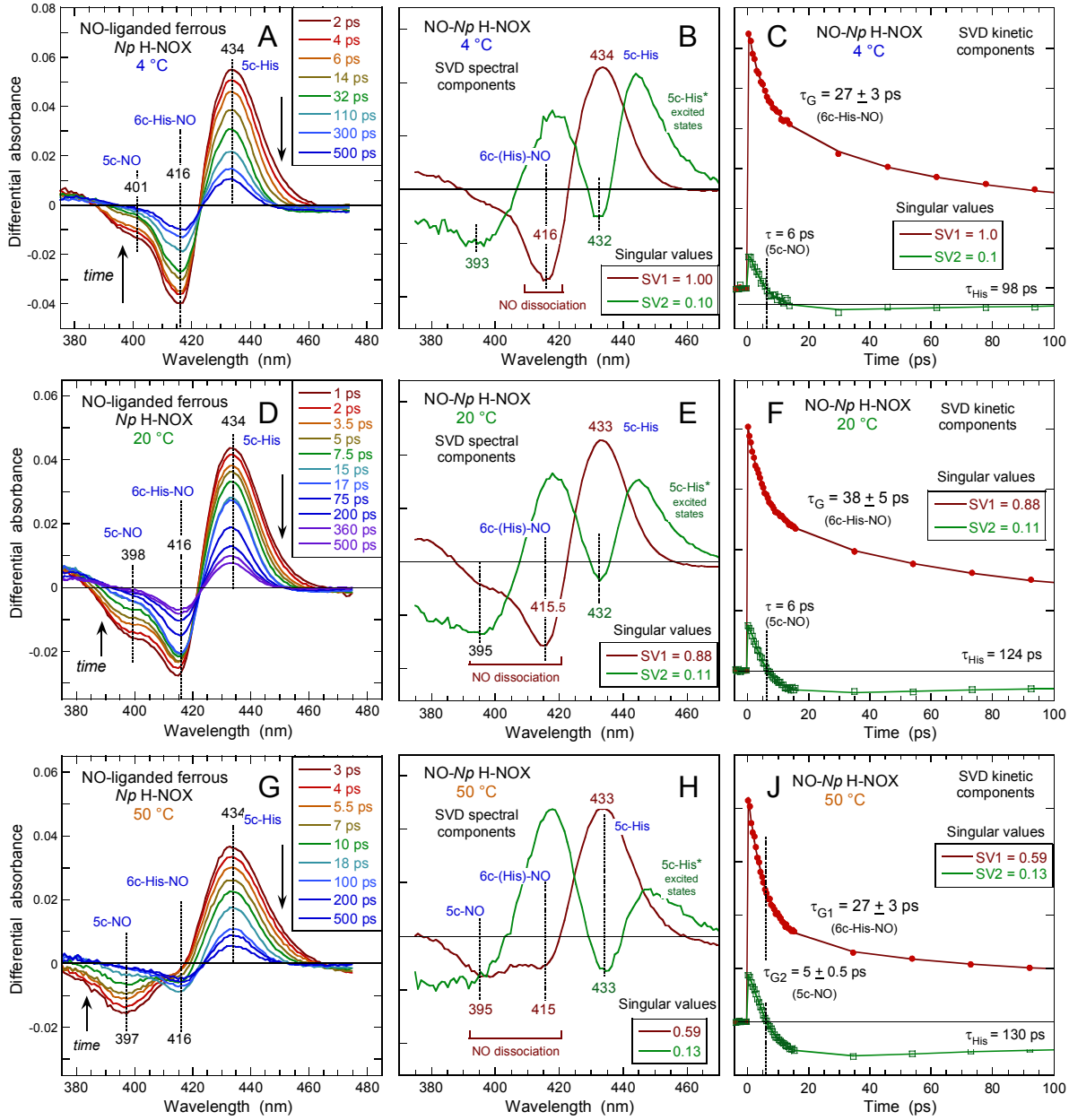

Figure S7. Interaction of NO with *Np* H-NOX at increasing temperature (4, 20 and 50 °C). **A, D G**: Raw transient spectra a selected time delays after NO photodissociation. **B, E, H**: Spectral components from the SVD analysis of the time-wavelength matrix. **C, F, J**: Associated SVD kinetic components describing the evolution of the SVD spectral components.

Table S2. Parameters of the fit of the SVD kinetic components for *Np* H-NOX.

T	SVD Comp.	Singular value	5c-NO τ_5 (A_5)	6c-(His)-NO		τ_{His} (A_H)	constant (A_C)
				τ_6 (A_6)	τ'_6 (A'_6)		
4 °C	SVD1	1.00	5.6 ps (*0.31*)	32 ps (*0.22*)	290 ps (*0.35*)	–	*0.12*
	SVD2	0.10	6.1 ps (*0.73*)	–	–	99 ps (*0.12*)	*0.15*
20 °C	SVD1	0.88	4.9 ps (*0.36*)	38 ps (*0.20*)	309 ps (*0.33*)	–	*0.11*
	SVD2	0.11	5.2 ps (*0.78*)	–	–	124 ps (*0.12*)	*0.11*
50 °C	SVD1	0.59	5.8 ps (*0.56*)	36 ps (*0.13*)	305 ps (*0.21*)	–	*0.10*
	SVD2	0.13	5.9 ps (*0.74*)	–	–	130 ps (*0.15*)	*0.11*

Time constants :
τ_5 = 5.6 ± 0.5 ps : NO geminate rebinding to the 4c heme to form 5c-NO.
τ_6 : NO geminate rebinding to the 5c-His heme to form 6c-(His)-NO.
τ_6 = 35 ± 3 ps : from within the heme pocket.
τ'_6 = 301 ± 15 ps : from the protein core.
τ_{His} = 118 ± 19 ps : Proximal Histidine rebinding to the 4c heme.
The constant term (A_C) corresponds to NO having not rebound after 500 ps.

The transient spectra have been measured at 4, 20 and 50 °C for *Np* H-NOX. At 4 °C the maximum of induced absorption is centered at 434 nm (5c-His) with a minimum of bleaching at 416 nm [6c-(His)-NO] and a very small contribution around 401 nm (5c-NO) (Fig. S6A). The shift of the isosbestic point (423 nm) appears extremely small and NO rebinding to 5c-His to form 6c-(His)-NO represents the predominent contribution. SVD calculation resulted in two individual spectral components (Fig. S6B and C), the first one corresponding to geminate recombination of NO to the heme 5c-His + NO → 6c-(His)-NO identified by the bleaching at 416 nm. The second one, SVD2, is attributed to a small contribution of NO and proximal His rebinding to the 4c heme formed by the dissociation of the initial 5c-NO species. At 20 °C, the proportion of 4c + NO → 5c-NO process increases in the SVD1 component (Table S2).

At 50 °C the transient spectra (Fig. S6G) have a very different evolution: a bleaching recovery in the early time (within 15 ps) is well marked at 397 nm, which implies a large proportion of 4c + NO → 5c-NO process and a second bleaching whose amplitude is smaller and decays more slowly after 15 ps.

The kinetics associated with SVD1 (Fig. S6C, F, J) were fitted to the sum of three exponential terms (Table S2). The fastest (5.6 ± 0.5 ps) is due to the 5c-NO species formation,

whereas the slower (32 ± 7 ps and 290 ± 28 ps) are due to the 6c-NO species formation. The singular values SVD1 and SVD2 can be compared together only at one temperature because they depend upon the absorption coefficient of the sample and experimental conditions. However, we can compare the ratio SVD1/SVD2 between temperatures. This ratio decreases as *T* is raised, showing the more important contribution of NO rebinding to the 4c heme and of the proximal His rebinding with increasing *T*. Their relative amplitudes clearly change.

NO dynamics in *Caldaneaerobacter tencongensis* H-NOX

Table S3. Time constants and relative amplitudes from fitting the SVD kinetic for *Ct* H-NOX.

T	SVD comp.	Singular value	τ_{ex} (A_{ex})	τ_G (A_G)	τ_R (A_R)	Constant (A_0)
20 °C	SVD1	0.950	3.6 ps (*0.48*)	–	15 ps (*0.18*)	*0.34*
	SVD2	0.506	–	7.3 ps (*0.78*)	–	*0.22*
74 °C	SVD1	0.703	2.1 ps (*0.29*)	–	9.2 ps (*0.45*)	*0.26*
	SVD2	0.572	–	7.0 ps (*0.81*)	–	*0.19*

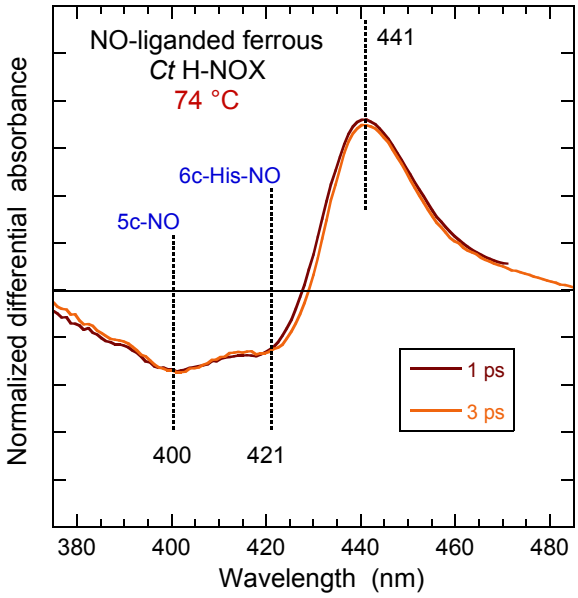

Figure S8. Comparison of the two raw transient spectra at +1 and +3 ps after NO photodissociation, normalized with respect to the minimum at 400 nm. The very small shift of the isosbestic point at ~428 nm is due to heme vibrational relaxation. The same shape of the bleaching part, especially the same negative intensity at 400 and 421 nm demonstrates the same time constant for both spectral component.

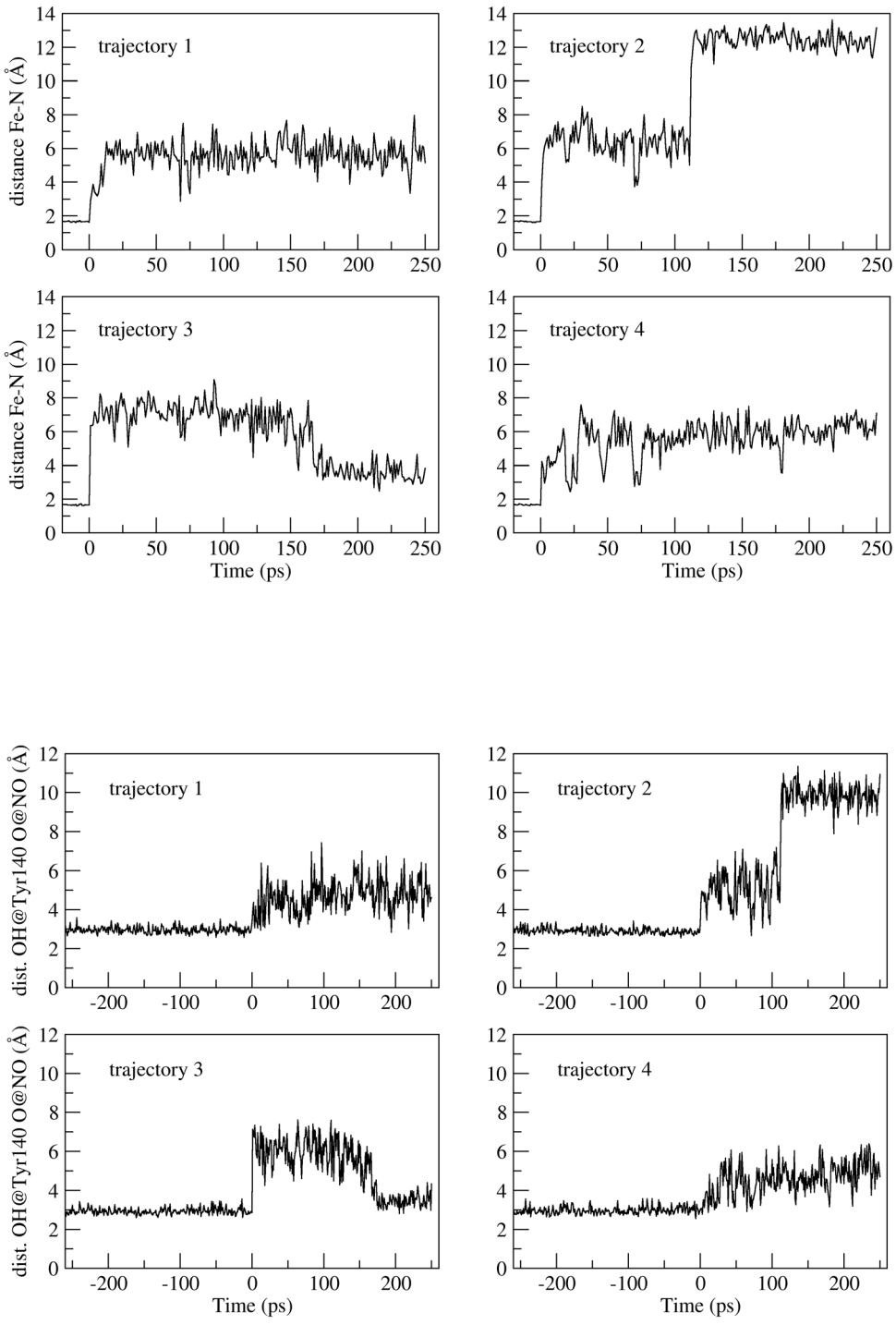

Figure S9. Four simulated trajectories of NO within the heme pocket of *Ct* H-NOX after NO dissociation from 6c-(His)-NO. The upper panels describe the evolution of the Fe-NO distance and the lower panels describe the Tyr140(OH)–ON distance. At steady state, the interaction between the hydroxyl of Tyr140 and the oxygen atom of NO forms a hydrogen bond whose distance is remarkably stable at ~3 Å during energy minimization phase (negative time in lower panels). These simulations are not intended to perform statistics, but to describe possible motions of photodissociated NO. The graphical time step is 1 ps, but was 1 fs for calculations.

Table S4. Affinities and binding rates from and to the solution for the H-NOX family.

Data from:

A.-L. Tsai, V. Berka, F. Martin, X. Ma, F. van den Akker, M. Fabian and J. S. Olson, *Biochemistry*, 2010, **49**, 6587−6599.

G. Wu, W. Liu, V. Berka and A.-L. Tsai, *Biochemistry*, 2015, **54**, 7098−7109.

H-NOX	NO			CO			O_2		
	k_{on}	k_{off}	K_D	k_{on}	k_{off}	K_D	k_{on}	k_{off}	K_D
	$M^{-1} \cdot s^{-1}$	s^{-1}	M	$M^{-1} \cdot s^{-1}$	s^{-1}	M	$M^{-1} \cdot s^{-1}$	s^{-1}	M
Cb	1.5×10^{8}	1.2×10^{-2}	8×10^{-11}	1.5×10^{6}	1	7×10^{-7}	–	~2500	5×10^{-5}
Np	3×10^{8}	0.05	2×10^{-10}	3×10^{6}	3.6	1.4×10^{-6}	autoxydation		
Ct	1.5×10^{8}	3×10^{-3}	2×10^{-11}	4×10^{6}	0.5	1.6×10^{-7}	2×10^{7}	1.2	9×10^{-8}
sGC	2×10^{8}	6×10^{-4}	3×10^{-12}	4×10^{4}	~11	2.6×10^{-4}	sGC does not bind O_2		

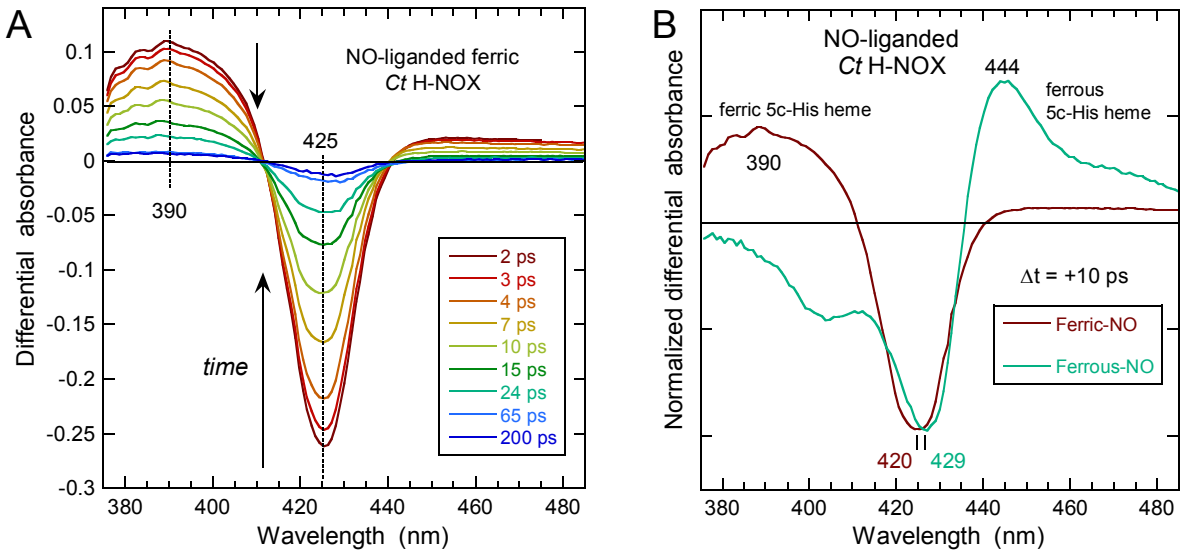

Figure S10. A: Transient spectra of NO-liganded ferric *Ct* H-NOX at various time delays. Only one process is detected, NO geminate recombination, as witnessed by the fixed position of the two isosbestic points (412 and 441 nm). **B**: Comparison of normalized transient spectra at Δt = +10 ps for ferrous and ferric *Ct* H-NOX. The absence of the broad induced band at 390 nm in the case of ferrous sample allows to discard the hypothesis of heme photo-oxidation.

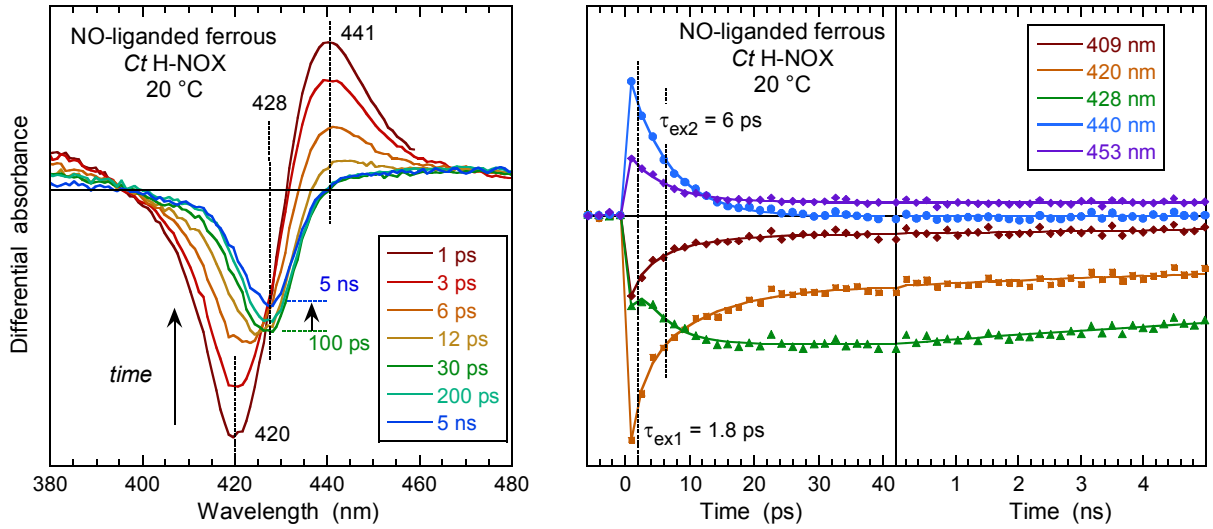

Figure S11. Dynamics of *Ct* H-NOX heme after NO photodissociation up to 5 ns. **A**: Transient spectra. **B**: Kinetics at particular wavelengths.

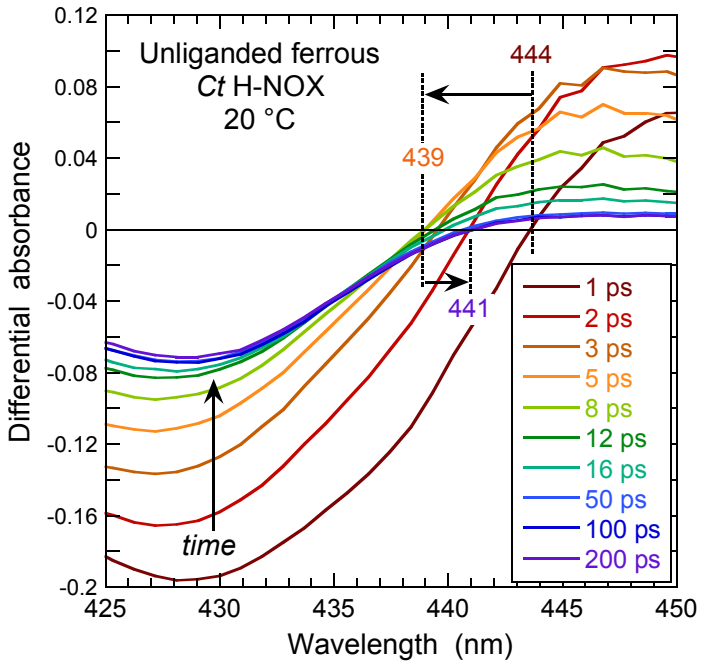

Figure S12. Shift of the isosbestic point after photo-excitation of unliganded ferrous *Ct* H-NOX. The first shift from 444 to 439 nm is due to excited states dynamics, whereas the second one from 439 to 441 nm reveals heme structural relaxation associated with the decay of the bleaching at 428 nm.

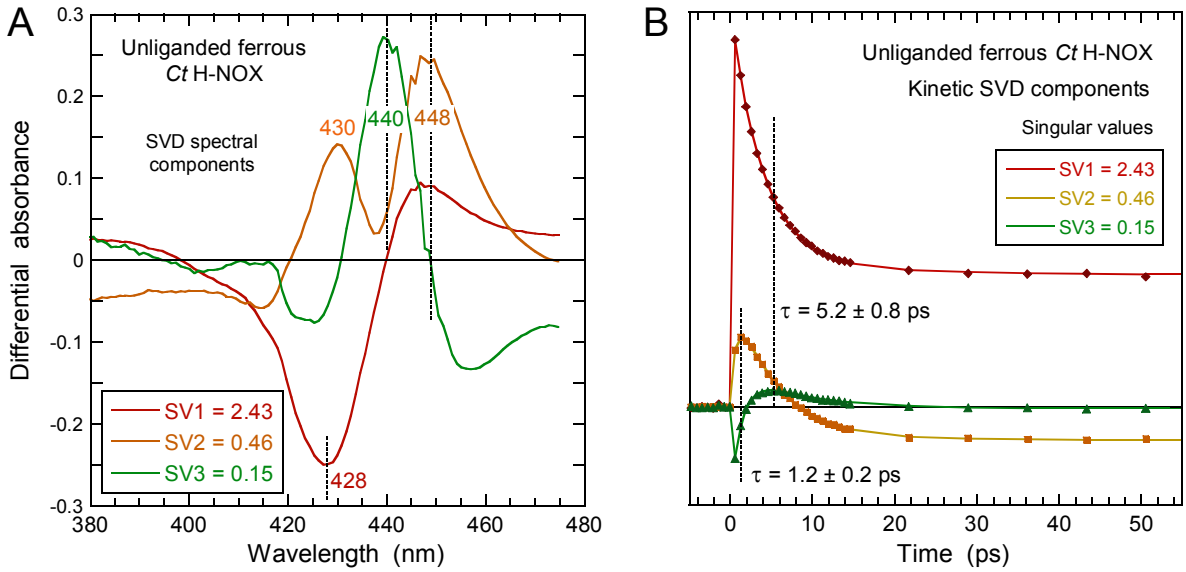

Figure S13. Excited states dynamics of ferrous unliganded *Ct* H-NOX. **A**: Spectral components from Singular Value Decomposition of the time-wavelength data matrix in Figure 6A. The relative absorbance is obtained by multiplying with the respective singular value. **B**: SVD kinetic components with time constants of the fitted exponentials. The SVD components correspond to 1- the decay of the initial electronic excited state to the second one (τ_{ex1} = 1.2 ± 0.2 ps); 2- the relaxation from the second excited species to a less distorted heme (τ_{ex2} = 5.2 ± 0.8 ps). The intermediate species (formed in 1.2 ps) has a spectrum centered at 440 nm and decays to the relaxed heme whose spectrum is centered at 435 nm (Fig. 6C).

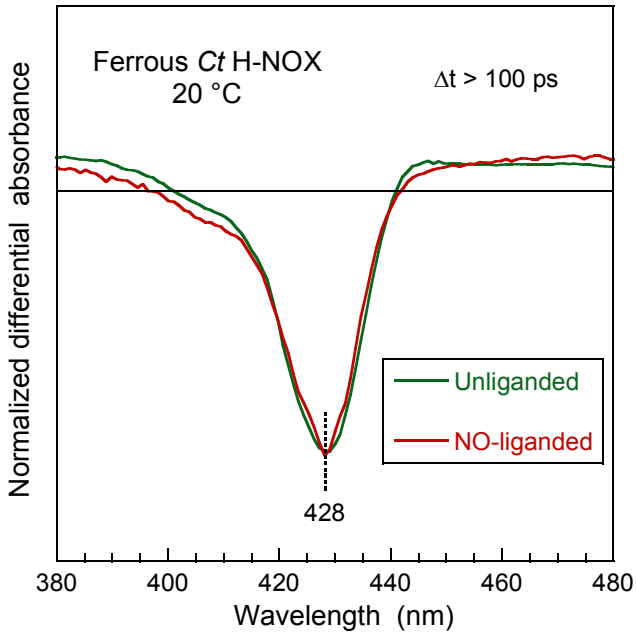

Figure S14. Comparison of the differential spectra at time Δt > 100 ps from unliganded and NO-liganded ferrous *Ct* H-NOX.

Table S5. Raman bands assignments and frequencies (cm^{-1}) in CW spectra in Figures 7 and S15.

Mode assignment	Ferrous *Np* H-NOX	Ferrous *Np* H-NOX–NO	Ferrous *Ct* H-NOX	Ferrous *Ct* H-NOX–NO
ν(Fe–His)	208	–	216	–
ν_9	275	280	275	–
γ_7 [γ(C–C)]	302	–	296	–
γ_6	317	324	–	–
ν_8	346	345	349	347
δ(C–C–C) prop.	372	375 (w)*	373	376
$\delta(C_\beta–C–C)$ vinyl	420	429	416	419
γ_{12}	494	480	489	–
γ_{21}	weak	shoulder	546	538 (w)
ν(Fe–NO)	–	551	–	553
ν_{48}	586	–	585	–
ν_7	678	679	674	677
γ_{11} (+γ_{15})	709	713	707	707
ν_{15}	755	756	759	754
ν_6	790	795 (w)	785	790 (w)
Phe ring breathing	997	1001	1003	1001
ν_5	1118	1123	1117	1118
ν_{14}	1133	1136	1133	1135
ν_{30}	1191	–	1184	1178
ν_{13} [+ $\delta(CH_2)$]	1213 - 1225	1224	1219	1225
δ(C–H)	–	–	1243 (w sh)*	shoulder
ν_{21} + δ(C–H)	1304	1306	1306	1306
ν_4	1357	1374	1354	1372
$\delta(CH_2)$	1421	1434	1425	1432
ν_{28}	overlapped with ν_3	1465	overlapped with ν_3	1465
ν_3	1472	1501 - 1505	1470	1497 - 1509
ν_{38}	1523	–	–	–
ν_{11}	shoulder	1554	shoulder	1560
ν_2	1564	1581	1566	1581
ν_{37}	1589	–	1586	shoulder
ν(C=C) in plane	1605	1605	1603	–
ν(C=C) vinyl + ν_{10} (6c heme)	1625	1634	1620	1625
ν_{10} (5c-NO heme)	–	1645	–	1645

* w: weak band; sh: shoulder.

The Raman bands assignments in Table S5 were performed after:

S. Choi and T. G. Spiro, Out-of-plane deformation modes in the resonance Raman spectra of metalloporphyrins and heme proteins. *J. Am. Chem. Soc.*, 1983, **105**, 3683–3692.

T. G. Spiro and X.-Y. Li, Resonance Raman spectroscopy of metalloporphyrins, *in Biological Applications of Raman Spectroscopy: Resonance Raman Spectra of Heme and Metalloproteins* Vol. **3** (Spiro, T. G., Ed.) pp 1–37, (1988) John Wiley & Sons, New York.

S. Hu, I. K. Morris, J. P. Singh, K. M. Smith and T. G. Spiro, Complete assignment of cytochrome c resonance Raman spectra via enzymatic reconstitution with isotopically labeled hemes. *J. Am. Chem. Soc.*, 1993, **115**, 12446–12458.

S. Hu, K. M. Smith and T. G. Spiro, Assignment of protoheme resonance Raman spectrum by heme labelling in myoglobin. *J. Am. Chem. Soc.*, 1996, **118**, 1638–12646.

C. Le Moigne, B. Schoepp, S. Othman, A. Verméglio and A. Desbois, Distinct structures and environments for the three hemes of the cytochrome bc(1) complex from *Rhodospirillum rubrum*. A resonance Raman study using B-band excitations. *Biochemistry*, 1999, **38**, 1066–1076.

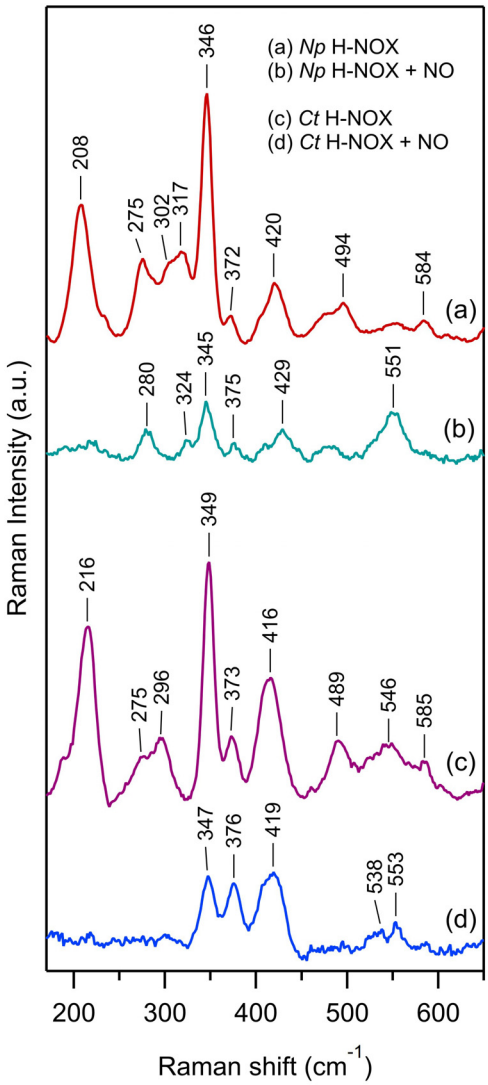

Figure S15. Enlarged view of the low frequency range of CW Raman spectra of *Np* and *Ct* H-NOX.

EXPERIMENTAL METHODS

Protein expression and preparation

The H-NOX domains of proteins from three different bacteria were overexpressed in *E. coli* as already described.[1] His-tagged H-NOX (1-186) from *Clostridium botulinum*, H-NOX (1-183) from *Nostoc punctiforme* and H-NOX (1-191) from *Caldanaerobacter subterraneus tengcongensis* were purified by nickel affinity chromatography followed by gel filtration. The produced proteins were > 98 % pure as determined by gel electrophoresis. Bovine (*Bos taurus*) soluble guanylate cyclase was purified from beef lung as previously described.[2]

For the spectroscopic measurements, 90 µL of protein solution were placed in a quartz cell (1-mm optical path, Hellma) and degassed with three cycles of vaccum/argon. To fully reduce the H-NOXs, we introduced a 10-µL aliquot of degased sodium dithionite $Na_2S_2O_4$ (5 mM) into the cell containing argon with a gastight syringe to obtain final concentration of 0.5 mM. However, *Ct* H-NOX is purified in the ferrous O_2-liganded form and O_2 cannot be removed by merely degasing the solution due to its very high affinity. It was necessary to briefly heat the cell under Ar at 70 °C (~2 minutes in a water bath) in order to displace O_2. This procedure induced partial oxidation of *Ct* H-NOX which was reduced by sodium dithionite. The heating step was not necessary for *Cb* and *Np* H-NOX.

The formation of NO-liganded *Cb*, *Ct* and *Np* H-NOX was done by directly puting 10 % NO diluted in Ar into the cell through the gas train at a total pressure of 1.3 bar (~200 µM in the aqueous phase). The static and transient absorption for each H-NOX was measured as a function of temperature by means of a thermostated cell holder whose temperature was monitored with a thermocouple. The reduction and full equilibration with NO were verified by recording steady-state spectra at each step (Shimadzu UV-1700). The absorbance of the nitrosylated H-NOXs was in the range 0.4 to 0.6 at the Soret maximum for 1 mm path length.

Time-resolved absorption spectroscopy

Transient absorption measurements were performed with the pump-probe laser system previously described.[2] The ultra-short photo-dissociating and probing pulses were generated at a repetition rate of 30 Hz and have a duration of ~50 fs. The photodissociation of NO was achieved with a pulse at 564 nm (by excitation in the $Q_{0\text{-}0}$ band of the heme) whereas a white light continuum was used for obtaining a broad band probe pulse (375 – 550 nm). Both beams were focused to a spot of ~50 μm and spatially overlapped in the sample cell, which was continuously moved perpendicularly to the beams to ensure sample renewal between the laser

shots. The transient absorption spectra after a variable delay between pump and probe pulses were recorded with a liquid nitrogen cooled matrix CCD detector (~0.9 nm per pixel). Importantly, a reference beam was simultaneously recorded in another track of the detector. Up to 50 scans were recorded and averaged with a dwell time of 1 s at each time point.

Analysis of the data

Since we recorded a series of transient spectra at different time delays, the resulting data consists of a matrix of differential absorption as a function of time and wavelength. The global analysis of data was performed by singular value decomposition (SVD) of the matrix to identify all global spectral and kinetic dependencies by using the software Glotaran.[3]

The experimental time-wavelength data matrix $\Delta A(\lambda,t)$ of differential transient absorption spectra was decomposed according to:[4] $\Delta A(\lambda,t) = \Delta A^{SVD}(\lambda)\, S\, K^{SVD}(t)$ giving the orthogonal spectral component matrix $\Delta A^{SVD}(\lambda)$ and their associated kinetics matrix $K^{SVD}(t)$ weighted according to the singular values S_i (elements of the diagonal matrix S). SVD kinetics represent the evolution of the associated differential spectra. The assignment of the SVD components were based on the SDV spectra which allowed to identified the underlining process. A SVD component may contain the contribution of several transitions due to large overlapping of the spectra of species.

See detailed analysis below in ***Appendix 1***.

The singular values of the two major SVD components are presented together with kinetics $K^{SVD}(t)$ and spectra $\Delta A^{SVD}(\lambda)$. Other SVD component of much lower singular values were negligible and not taken into account for further analysis. The individual kinetic components $K_j^{SVD}(t)$ were fitted to a multiexponential function: $f(t) = \sum_i A_i \exp(-k_i t) + cst$ where the minimal number *i* of exponentials was determined iteratively. A non-zero asymptotic value (cst) can be included in some fits.

A reference pulse (same energy and spectrum as the probe pulse) is simultaneously recorded, allowing to calculate the absolute absorbance at each wavelength and time delay. Because photoexcitation is performed in non saturating conditions, there is a contribution from non photodissociated nitrosylated heme (~90 %) which can be removed by subtracting the spectrum before excitation with a weighting coefficient (~0.9) from the spectrum at a given time delay. We could thus obtain the pure absolute spectrum of the relaxed heme (Fig. 6B), whereas raw transient spectra are presented as differences to clearly show the changes.

Steady-state resonance Raman spectra

Resonance Raman spectra with continuous wave (CW) excitation were recorded using a He-Cd laser and the same Raman setup as for TR^3 studies.[5] The excitation wavelength of 441.6 nm has been chosen to closely match the probe beam wavelength (435 nm) in TR^3 measurements. The samples were contained in a spinning cylindrical quartz cell whose rotation speed was adjusted to produce a thin sample layer at the inner wall and to assure the absence of noticeable photoinduced changes in the spectra of nitrosylated complexes. The spinning cell was closed with a rubber stopper and degased the same way as used for the 1-mm cell in absorption experiments and filled either with Ar or NO 10 % diluted in Ar. The spectral resolution was estimated better than 5 cm^{-1}.

Time-resolved resonance Raman spectroscopy

Time-resolved sub-picosecond Raman apparatus has been described in detail elsewhere.[5] Briefly, it is based on a femtosecond Ti:Sapphire oscillator and a regenerative amplifier (output beam parameters are: wavelength 810 nm, pulse energy ~0.6 mJ, pulse duration 100 fs, repetition rate 1 kHz) and has 0.7-ps temporal resolution and 25-cm^{-1} spectral resolution. An optical parametric generator and two optical parametric amplifiers allowed to generate the photodissociating pump pulse (560 – 570 nm; 2 μJ; ~100 fs), whose delay was controlled by a translation stage, and the Raman probe pulse (435 nm; 25 nJ; 0.7 ps duration; 25 cm^{-1} spectral width). Both beams were collinearly overlapped by a dichroic mirror. Sample illumination and signal detection were performed in a 90° geometry, with excitation coming from the bottom of the spinning cylindrical quartz cell. The detection was performed with a liquid-nitrogen cooled back-illuminated CCD (Princeton Instruments SPEC-10 100BR/LN) at the output of a 1-m focal length spectrometer (Jobin-Yvon HR1000). Raman frequency calibration was performed using Kr and Xe spectral lamps (Oriel) and verified by recorded the spectrum of pure toluene. Absolute accuracy was ±2 cm^{-1} and relative accuracy ±1 cm^{-1}.

To obtain the pure photoproduct spectra from raw TR^3 data, we subtracted the weighted spectrum of the non-photoexcited protein (–5 ps) from that at + 2 ps to remove the contribution of 6c-(His)-NO ground state heme, as described in detail elsewhere.[4] All Raman spectra presented were corrected for the slowly changing background due to Rayleigh scattering and residual fluorescence using a cubic spline interpolation with Igor Pro software.

Ct H-NOX NO dynamic simulations

We constructed a model of the NO-liganded H-NOX protein from *Caldanaerobacter subterraneus subsp. tengcongensis* using the PDB file 3tf0 as a starting structure,[6] replacing the oxygen molecule with a NO ligand. The missing amino acids were constructed and added, and the entire structure was placed in a rhombic dodecahedron water box with a unit cell dimension of 83.6 Å. K^+ and Cl^- ions were added to cancel the total charge and simulate an ionic environment. The model consists of a polypeptide chain of 188 amino acids, a heme, a NO ligand, 12103 water molecules, 42 Cl^- ions and 41 K^+ ions, *i.e.*, a total of 39595 atoms.

Molecular dynamic simulations were performed using CHARMM software[7] version 36. Periodic boundary conditions were assumed and the particle mesh Ewald method was used to compute efficiently all long range electrostatic interactions. After an energy minimization step, the temperature of the structure was gradually increased from 110 K to 310 K for 100 ps, equilibrated at constant pressure for 250 ps, and then at constant volume for 1 ns. After a free dynamics of 250 ps, the NO molecule was dissociated from the heme iron atom, free to evolve within the protein structure (NO recombination to iron atom was not simulated). A three-charge model is used to simulate the dipole and quadrupole moments of the dissociated NO molecule. Four simulations of the NO dissociation and dynamics over 250 ps were performed using different initial starting equilibrated structures. An integration step of 1 fs was used and the coordinates of the structure were saved each 1 ps for further analysis.

1. P. Nioche, V. Berka, J. Vipond, N. Minton, A.-L. Tsai and C. S. Raman, Femtomolar sensitivity of a NO sensor from *Clostridium botulinum*. *Science*, 2004, **306**, 1550−1553.
2. M. Negrerie, L. Bouzhir, J. L. Martin and U. Liebl, Control of nitric oxide dynamics by guanylate cyclase in its activated state. *J. Biol. Chem.*, 2001, **276**, 46815−46821.
3. J. J. Snellenburg, S. Laptenok, R. Seger, K. M. Mullen and I. H. M. van Stokkum, Glotaran: a Java-based graphical user interface for the R package TIMP. *J. Stat. Softw.*, 2012, **49**, 1−22.
4. W. H. Press, B. P. Flannery, S. A. Teukolsky and W. T. Vetterling, *Numerical Recipes*, Cambridge University Press: New York (1989).
5. S. G. Kruglik, J.-C. Lambry, J.-L. Martin, M. H. Vos and M. Negrerie, Sub-picosecond Raman spectrometer for time-resolved studies of structural dynamics in heme proteins. *J. Raman Spectrosc.*, 2011, **42**, 265−275.
6. M. B. Winter, M. A. Herzik, J. Kuriyan and M. A. Marletta, Tunnels modulate ligand flux in a heme nitric oxide/oxygen binding (H-NOX) domain. *Proc. Natl. Acad. Sci. U.S.A.*, 2011, **108**, E881–E889.
7. B. R. Brooks *et al.* CHARMM: The biomolecular simulation program. *J. Comput. Chem*, 2009, **30**, 1545–1614.

Appendix 1

Global analysis of the time × wavelength data matrix.

Because the number of spectral SVD components with significant singular value is small (two for each data set) they contain the features of the raw data and we were able to attribute them to real processes. This assignment was allowed by the conpicuous similarity between the raw and SVD spectra. However, a full global analysis is mandatory to ensure that the SVD spectra presented in the main article correctly describe the real processes. In this purpose we have used the software *Glotaran*.

[Snellenburg, J. J., Laptenok, S., Seger, R., Mullen, K. M., & van Stokkum, I. H. M.
Glotaran: A Java-Based Graphical User Interface for the R Package TIMP.
Journal of Statistical Software, 2012, **49**, 1–22]

The spectra associated with each particular time constant and process were calculated from the SVD components. The most relevant model is parallel since the 4c heme (from photodissociated 5c-NO species) may evolve either to the original 5c-NO bound heme or to the 5c-His heme by proximal His rebinding. Because the initial proportion of 5c-NO and 6c-NO depends on the temperature there exist two simultaneous processes which do not interfer, as illustrated below for *Cb* and *Np* H-NOX proteins. In these schemes, "A" is the species before NO dissociation and hν represents the dissociating photon. The proportion of each process is indicated for each temperature.

Cb H-NOX :

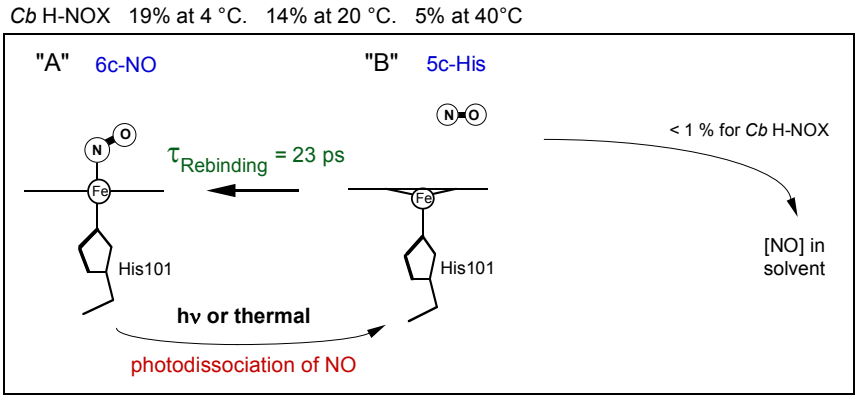

and :

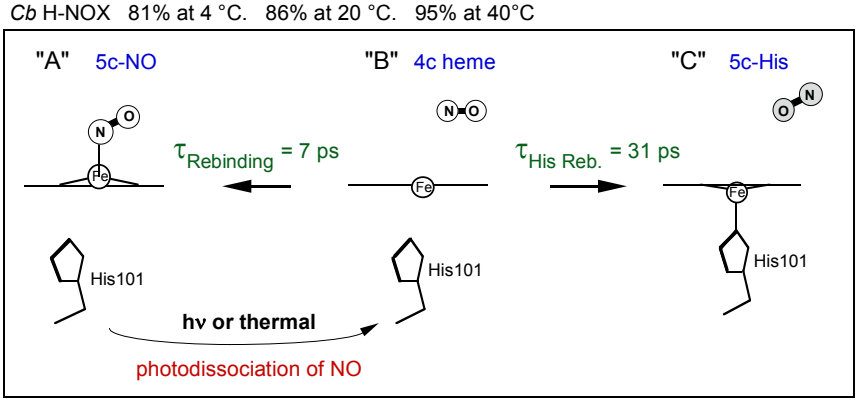

For *Cb* H-NOX at 40 °C the decay associated spectra obtained from global analysis are :

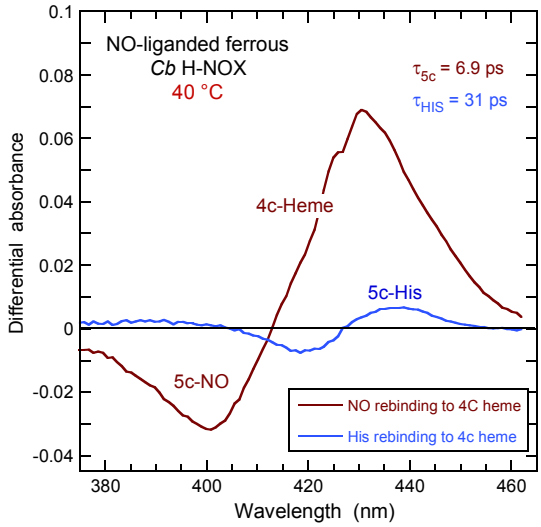

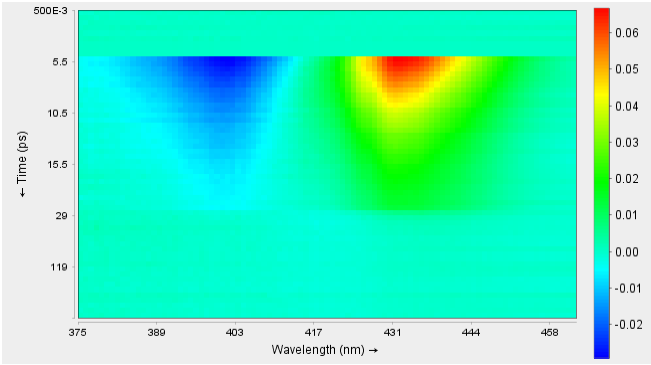

As demonstrated in the case of *Cb* H-NOX at 40 °C, the rebinding of the proximal Histidine is clearly identified by global analysis because the nitrosylated heme is almost entirely 5c-NO and its photodissociation leads to a 4c heme. The population evolution is described by the following kinetics, with 5c-NO and 6c-NO occuring simultaneously and whose relative amplitudes change as a function of temperature.

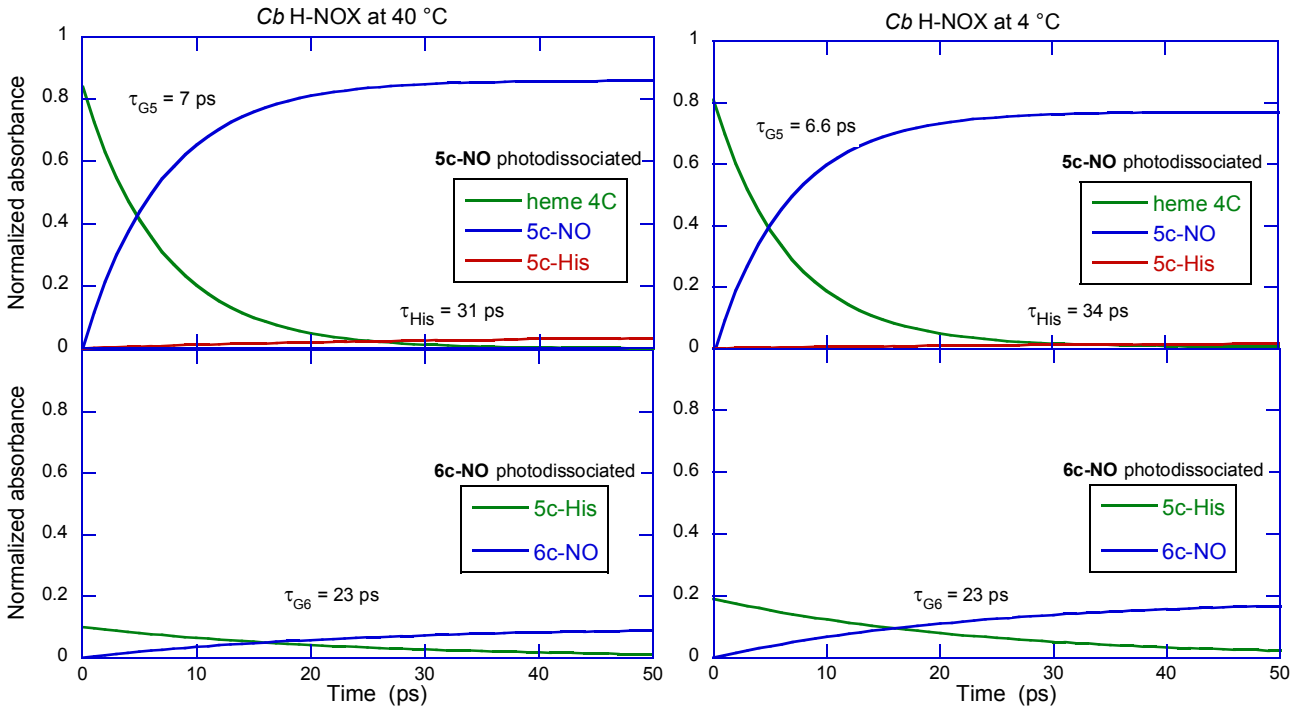

Np H-NOX :

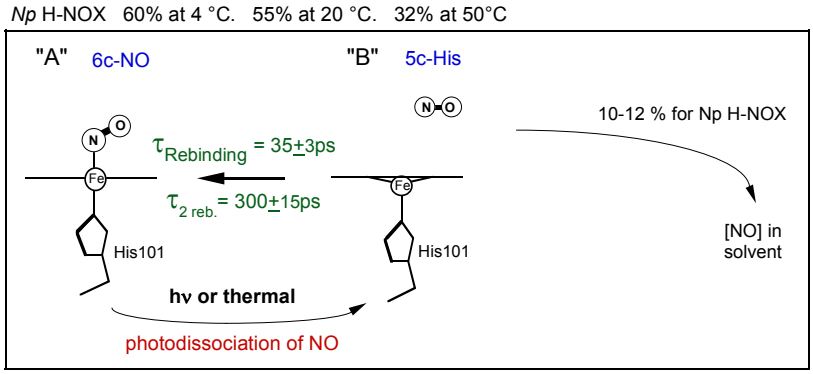

and :

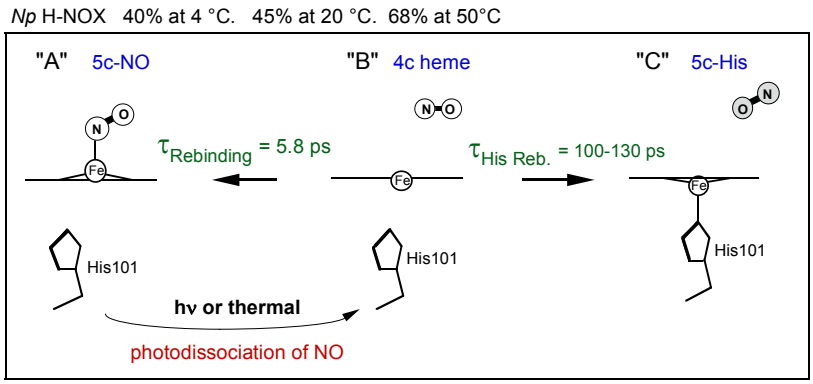

A global analysis yields a similar result for *Np* H-NOX protein at 50 °C with the presence of both 5c-NO and 6c-NO independent reformation as shown by the decay associated spectra :

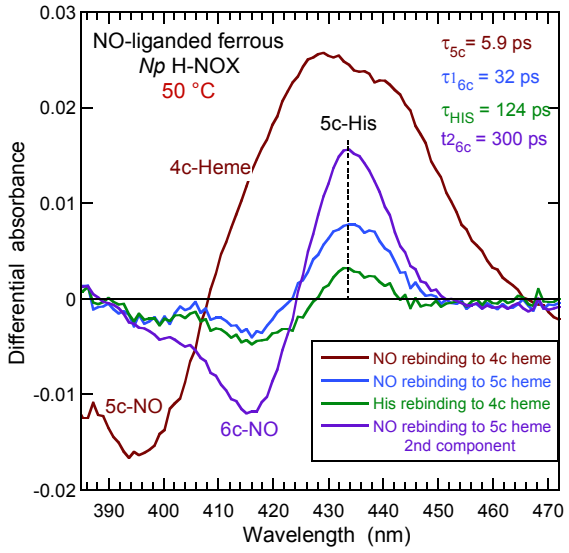

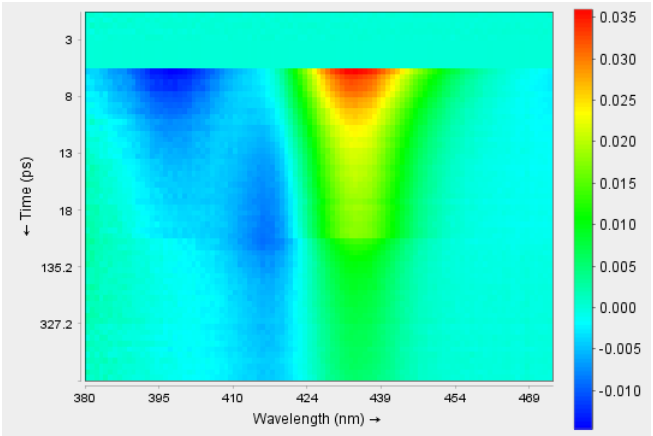

The relative amplitudes of 5c-NO and 6c-NO processes obviously change as a function of temperature :

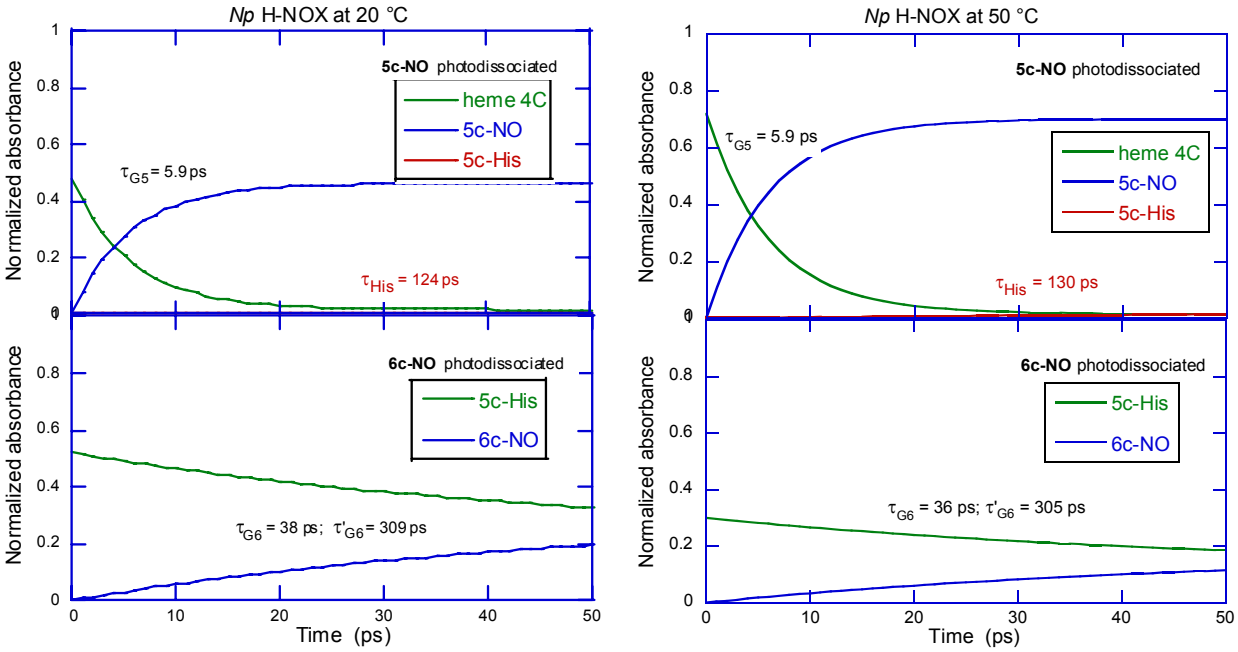

Ct H-NOX :

Ct H-NOX departs from the two other proteins by two remarkable features :

1- the heme is highly distorted (the most distorted one among all heme proteins) and this has pronounced effect on its dynamics.

2- one cannot separate 5c-NO and 6c-NO reformation processes because both have the same time constant (7 ps) and the spectra of the respective dissociated species, 4c and 5c-His, are very close to each other, broad and largely overlaped.

In Fig. 5A of the article the heme of *Ct* H-NOX is 6c-NO at 20 °C but yet fitting NO rebinding in this case (5c-His + NO → 6c-NO) results in a 7 ps-kinetics similarly with the case of 4c + NO → 5c-NO (to be compared to time constants in the range 12 – 24 ps for other proteins including non H-NOX like myoglobin).

Decay associated spectra obtained from global analysis at 74 °C :

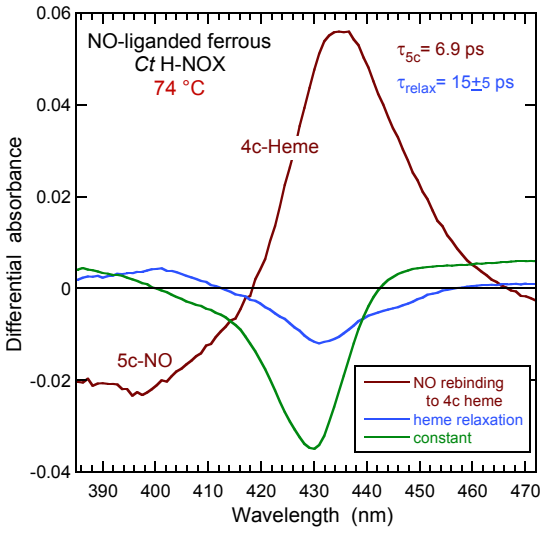

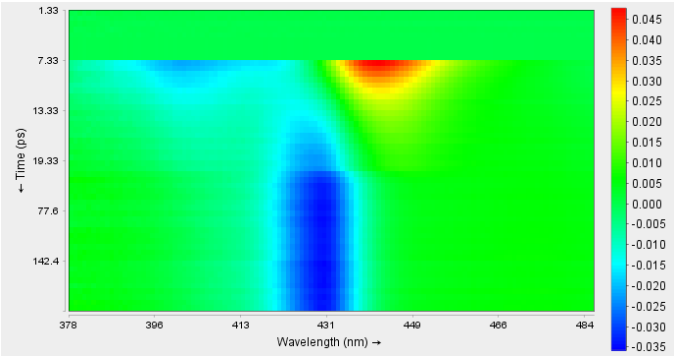

Ct H-NOX : 25% at 74 °C and >90% at 20°C

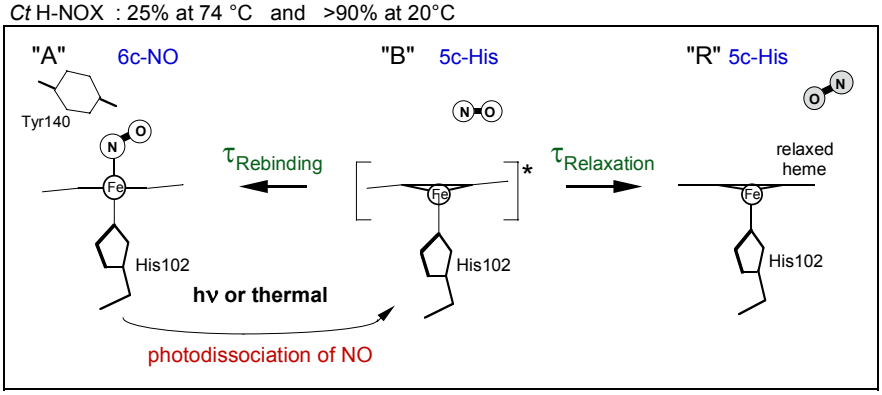

Ct H-NOX : 75% at 74 °C and <10% at 20°C

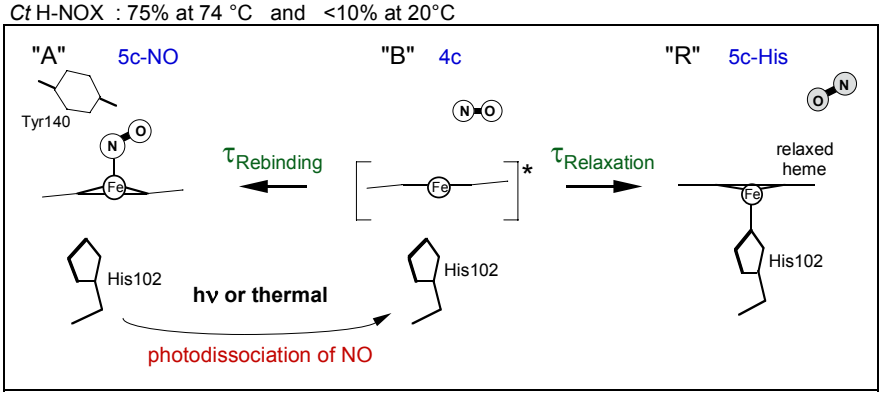

[]* denotes the unrelaxed distorted heme.

Heme relaxation occurs at both temperatures :

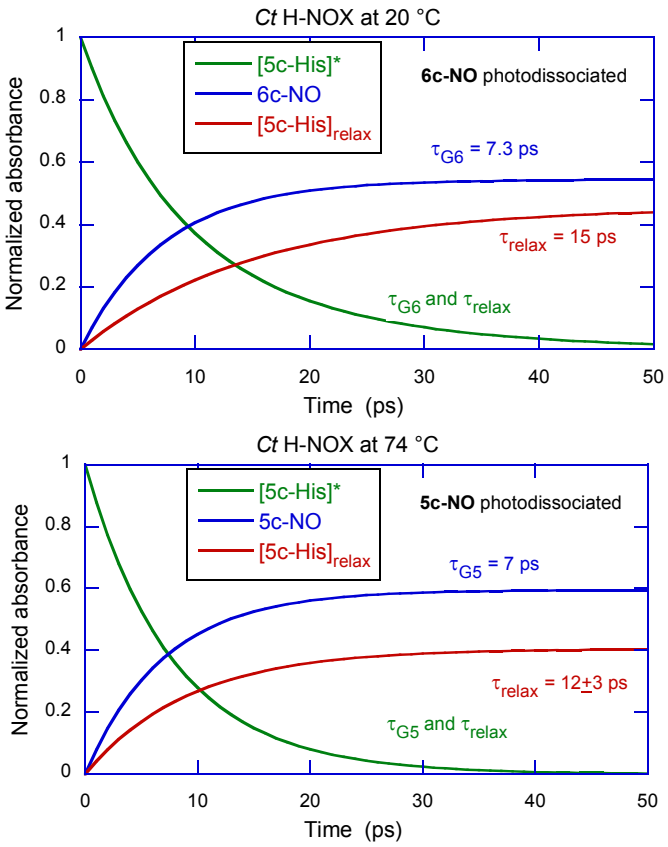
Ct H-NOX at 20 °C
[5c-His]*
6c-NO
[5c-His]relax
6c-NO photodissociated
τG6 = 7.3 ps
τrelax = 15 ps
τG6 and τrelax
Normalized absorbance
Time (ps)
Ct H-NOX at 74 °C
[5c-His]*
5c-NO
[5c-His]relax
5c-NO photodissociated
τG5 = 7 ps
τrelax = 12±3 ps
τG5 and τrelax
Normalized absorbance
Time (ps)